

## Novel Computer Tomography image enhancement deep neural networks for asphalt mixtures



Handuo Yang<sup>a</sup>, Ju Huyan<sup>a,\*</sup>, Tao Ma<sup>a</sup>, Zheng Tong<sup>a</sup>, Chengjia Han<sup>a</sup>, Tianyan Xie<sup>b</sup>

<sup>a</sup> School of Transportation, Southeast University, 2# Southeast University Road, Jiangning District, Nanjing 211189, China

<sup>b</sup> School of foreign Language, Nanjing University, 163# Xianlin Avenue, Qixia District, Nanjing 210023, China

### ARTICLE INFO

#### Keywords:

Asphalt mixture  
CT image enhancement  
Deep learning  
Semantic feature  
Multiple tasks

### ABSTRACT

This paper aims to solve two significant problems observed in Computer Tomography(CT) asphalt mixture images, which are 1) low-quality CT image, and 2) low efficiency, by intelligent word embedding methods. The first model is called Asphalt Mixture CT Image Enhancement Network (AMCTEN), which is featured by ignoring the semantic loss, while the second model, AMCTEN+, is feature by considering semantic loss without requiring semantic information. Two models can be integrated to realize end-to-end real-application image enhancement. Experimental results show that peak signal to noise ratio of AMCTEN and AMCTEN + in the test set increased by 79.0 % and 66.4 %, structural similarity increased by 15.1 % and 13.3 %, and mean square error decreased by 97.5 % and 95.3 %, respectively. Analysis of semantic feature spaces generated by the two models indicate that word embedding can construct an effective semantic feature space, fusing the semantic features with image features can improve the image quality, and the proposed model has superiority in multiple image enhancement tasks.

### 1. Introduction

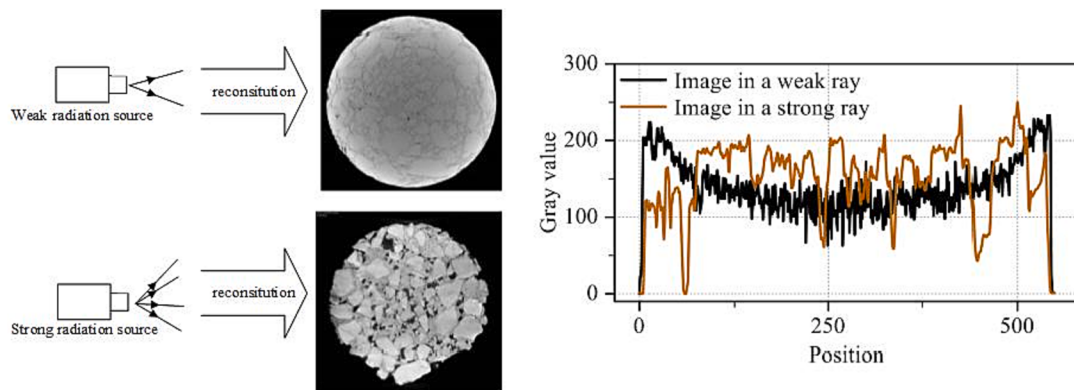
With the increased emphasize on green roads, green technologies, and sustainable development on transportation systems, researches on new technologies towards pavements, such as recycled pavement [1,2], drainage pavement [3,4], intelligent pavement detection technology [4,5] and intelligent compaction technologies have attracted the attention. As a kind of flexible pavement, the internal structure of asphalt mixture, such as gradation [6] and the homogeneity property of coarse aggregate skeleton [7] has important influence on the road performance. In order to improve the road performance of the pavement, the low-temperature cracking, fatigue cracking, rutting resistance and creep properties of asphalt pavements have been carried out over the last decades from the perspective of internal structure of the pavement [8,9].

Image technology, numerical simulation and sensor technology are the main methods for researchers to explore the internal structure of asphalt mixture. Image technology extracts internal structure information directly from asphalt mixture images [10], based on which to analyze the relationship between the internal structure and the control variables [11–15]. Huang et al. extracted the main axis direction of the

aggregate and the distance between layers from the image to evaluate the migration characteristics of porous asphalt concrete particle aggregates [16]. The research on the internal structure of asphalt mixture is also reflected in the numerical simulation [17]. Chen et al. reconstructed the three-dimensional structure of asphalt mixture voids and used it as a simulation input [18]. Du et al. established a local mean value model of asphalt mixture in combination with finite element. The proposed model considers both the global-scale pavement structure information and the local-scale internal structure information of the asphalt mixture [19]. With the help of sensors to detect internal structure response, it can reflect the impact of internal structure on road performance. Dan et al. used the Smart Rock sensor to obtain the internal stress during the compaction process to reflect the degree of compaction of the material [20]. Fu et al. used acoustic emission technology to detect internal damage during the loading process of asphalt mixtures, and studied the effects of freeze-thaw cycles and aging effects on damage [21]. Image technology is favored by more researchers due to its intuitiveness, convenience and easy access. However, image can only reflect the surface characteristic of the testing sample. To obtain more internal structure information, it is often necessary to further cut and photograph the sample. This method destroys the original sample and cannot

\* Corresponding author.

E-mail addresses: [230218945@seu.edu.cn](mailto:230218945@seu.edu.cn) (H. Yang), [jhuyan@seu.edu.cn](mailto:jhuyan@seu.edu.cn) (J. Huyan), [matao@seu.edu.cn](mailto:matao@seu.edu.cn) (T. Ma), [230208346@seu.edu.cn](mailto:230208346@seu.edu.cn) (C. Han).



**Fig. 1.** CT image comparison under different intensity rays.

achieve a high degree of three-dimensional restoration. Therefore, it is necessary to provide a non-destructive testing method to restore and three-dimensional reconstruction of the internal structure.

Computer Tomography (CT) technology, as a nondestructive testing technology, has been widely used for asphalt mixture analysis and achieved successful applications [22–24]. Cui et al. used CT technology to analyze the moisture damage mechanism, and pointed out the influence of water pressure on the degree of moisture damage [25]. When Xu et al. used CT technology to demonstrate the evolution of the internal structure of the asphalt mixture, and pointed out the main manifestations of the diversification of the internal structure [26]. Li et al. used CT to investigate and observe the internal structure changes of asphalt mixture during rotary compaction [27]. Li et al. also used CT imaging technology to determine the direction of the aggregate, the number of aggregate contact points, the void distribution and the void shape index [28]. In order to obtain the internal structure information, the researchers also combined a large number of digital image processing techniques to repair, segment and detect the edges of CT images [29]. By adding perlite powder, Wei, JJ et al. realizing the improvement of image segmentation accuracy from the perspective of asphalt mixture materials [30]. Zhang et al. used the ring block OTSU method to study the void distribution characteristics of asphalt mixture in combination with non-destructive testing technology [31]. Hu et al. used the same ring segmentation method to study the three-dimensional voids of asphalt mixtures [32]. Huang et al. used an improved morphological algorithm to segment the adhering parts of aggregates in asphalt mixtures [33]. Xing et al. accurately and effectively extracted the gradation information of AC, SMA and OGFC from CT images [34]. The use of traditional image processing methods for CT image processing requires a series of processing procedures and cumbersome threshold determination, which is a significant disadvantage when dealing with big datasets, for which the efficiency usually significantly decreased. In addition, traditional step-by-step processing methods usually have their own problems, such as local threshold segmentation has the incoherence problem between the local and the global. This indicates that more convenient and accurate image processing solution is required.

With the rise of deep learning technology, researchers have turned to the application of DL technologies in asphalt mixture images analysis with the objective of obtaining more comprehensive information from the images, thus making the analysis more intelligent [35–37]. Jiang et al. used the convolutional neural network to classify the CT scan images of asphalt mixtures, and realized the automatic recognition of different types of asphalt mixtures [37]. Aiming at the voids segmentation problem of CT images of asphalt mixture, Enriquez-Leon et al. compared various image segmentation techniques including deep learning. The results showed that machine learning and deep learning segmentation results are accurate [38]. These studies have made significant contributions to the intelligent classification and segmentation of asphalt mixture CT images. However those solutions are usually based

on traditional image enhancement methods when the quality of the image cannot meet the requirement [39,40], for example, Non-Local Network [41], DnCNN, and MWCNN [42]. This provides a new idea for researchers to solve the CT image enhancement problem of asphalt mixture. As the first step of image processing, image preprocessing plays a vital role in subsequent image processing and the correct characterization of the internal structure of the aggregate.

Therefore, an efficient, accurate, time-saving and laborsaving method is needed to improve the quality of CT images of asphalt mixtures. This research developed two models to solve the above-mentioned problems about CT image of asphalt mixture. Specifically, the first model, Asphalt Mixture CT Image Enhancement Network (AMCTEN), pays more attention to the improvement of repair quality, while the second model, AMCTEN+, is focused on the reduction of processing workload. The CT image data set of high-quality asphalt mixture are obtained by scanning samples in multiple angles and directions, by which the image restoration data set is constructed. Experimental results prove that AMCTEN can recognize semantic information, while AMCTEN+ can automatically recognize semantic information. The results of CT image enhancement of asphalt mixture were verified by Peak signal to noise ratio (PSNR), Structural similarity (SSIM), and mean square error (MSE) indicators. The results show that the model proposed in this study outperforms popular algorithms such as FCN.

## 2. Problem statement

### 2.1. CT scanning related problems

Generally, the difference between density components of asphalt mixtures, such as the voids, mortar and aggregates, are reflected by different brightness in the CT images. To this point, there are two key prerequisites for obtaining reliable results based on CT images, which are 1) being able to obtain high-precision images, and 2) work on multi-sourced images.

To date, the main obstacle of CT based asphalt mixture analysis is the low-quality phenomenon of, which are usually reflected in the following two aspects:

1. Variation in radiation sources related quality decrease. If the intensity of radiation does not match the mixture density, the captured asphalt mixture image becomes extremely dark or bright; and the noise generated in the process of imaging and transmission makes the image not smooth enough and reduces the image edge quality; the insufficient intensity of the ray can also bring the problem of blurred image and low image quality. Brightness, clarity, and noise issues will adversely affect subsequent analysis and calculations. As shown in Fig. 1, radiographic imaging quality of different intensities vary significantly. Insufficient radiographic intensity produces a

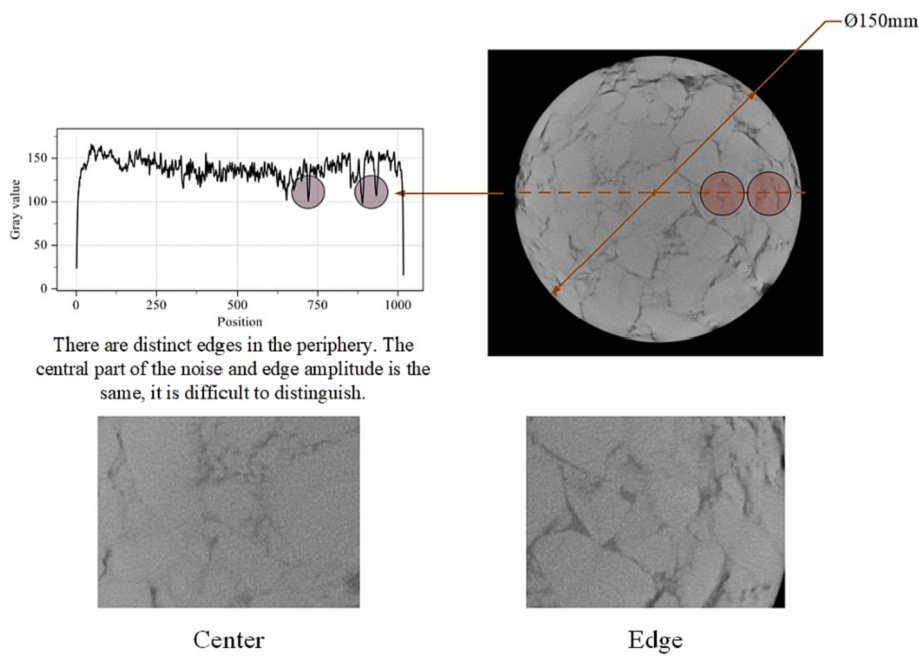


**Fig. 2.** Circumferential image quality of asphalt mixture samples.

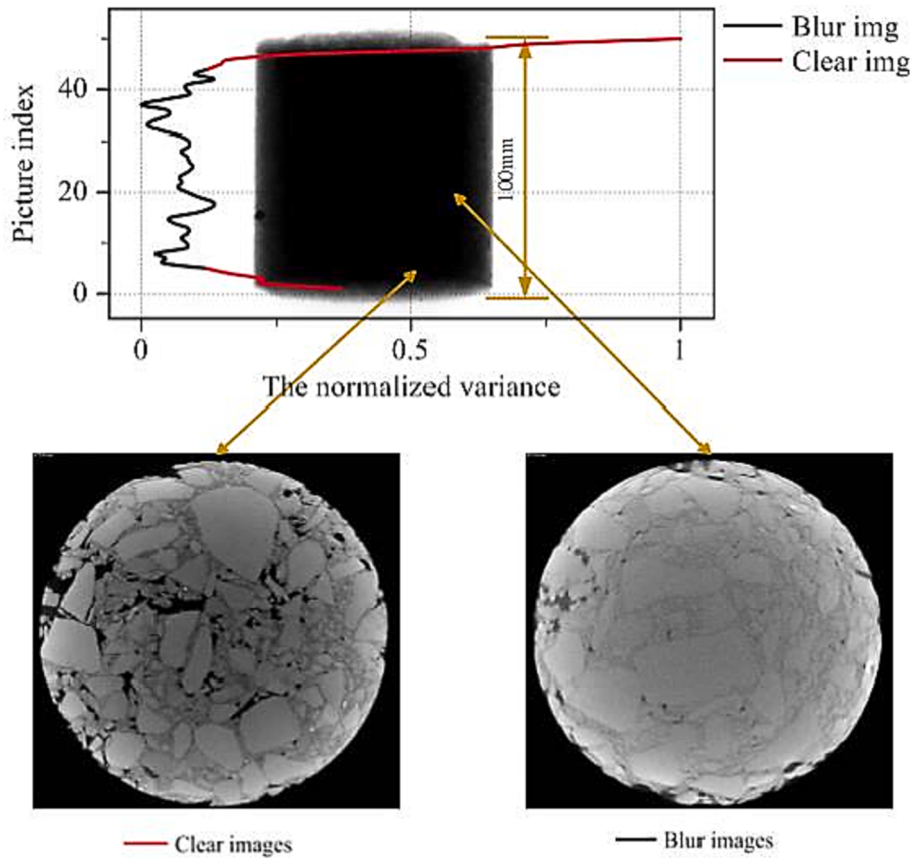


**Fig. 3.** Image quality in the height direction of asphalt mixture samples.

large amount of image noise, and image blurring leads to insufficient differentiation of internal noise and boundary.

2. Over thick sample with insufficient radiation source related quality decrease. In order to characterize the pavement structure, asphalt mixture specimens are often large in size, such as standard rutting

specimens ( $300\text{ mm} \times 300\text{ mm} \times 50\text{ mm}$ ), core specimens with a diameter greater than 100 mm. These large-size samples can also cause poor-quality images due to insufficient ray intensity, and images with sufficient sharpness and detailed information cannot be obtained. The scanning picture of core sample of pavement structure

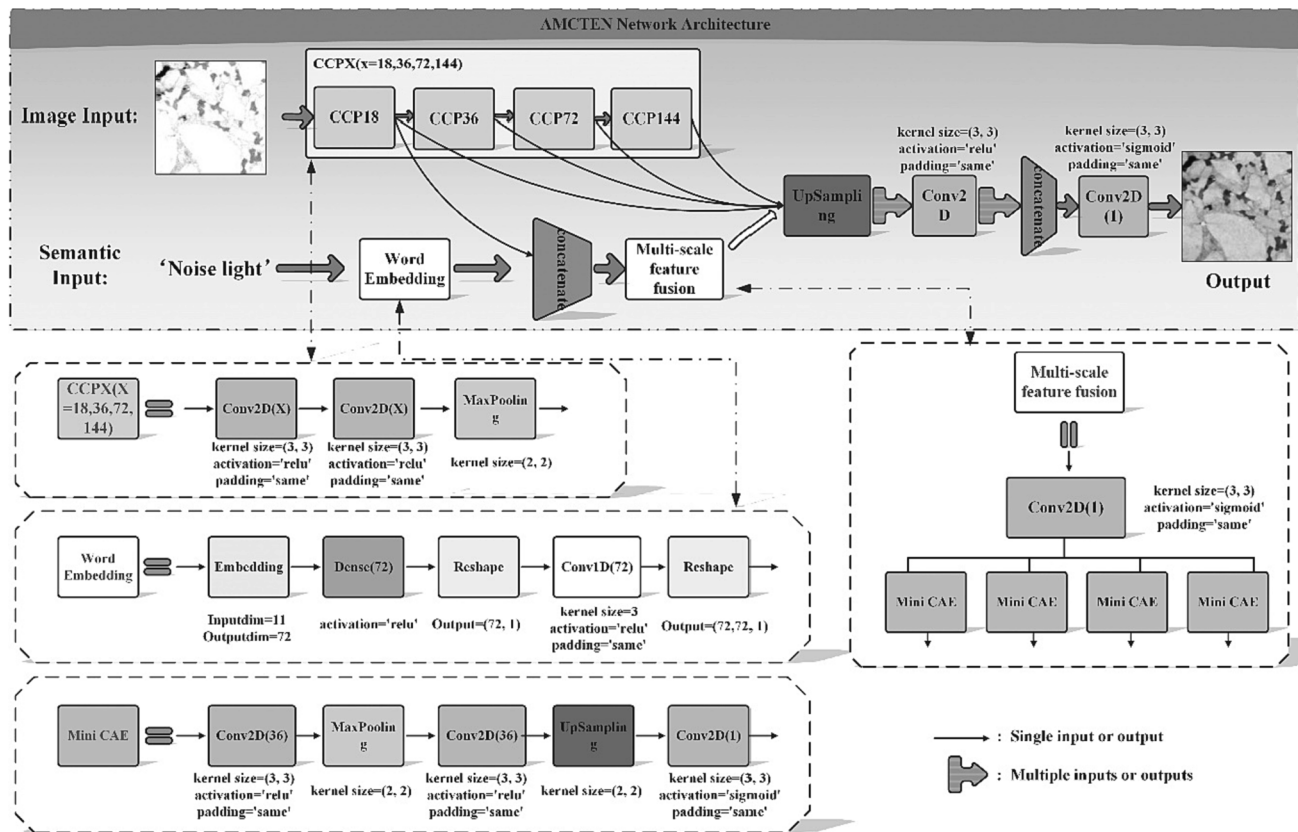


Fig. 4. AMCTEN network architecture.

with a diameter of 150 mm is shown in the Fig. 2. As can be seen from the Fig. 2, a large amount of edge information is lost due to the thickness of the sample and the insufficient radiation. In addition, slice images located at different heights can also have different imaging quality, as shown in the Fig. 3. It can be seen that the areas with large grayscale changes in the image indicate that the upper and lower ends of the sample contain more grayscale information.

In addition, in Fig. 3, the distinguishability of the bottom image aggregate is significantly better than the image information collected from the middle of the light. The above two situations reflect the law of attenuation from the outside to the inside of the asphalt mixture specimen. The reason for this phenomenon is that the material close to the outside becomes more easily penetrated due to the reduced distance of radiation penetration. In addition, the closer to the upper and lower ends, the greater the void content of the specimen it is. And therefore, the easier it is to be penetrated by rays. However, there are still valid information of internal structure in the image, so it is necessary to provide an appropriate image enhancement scheme to solve this problem.

In the solution of CT image enhancement of asphalt mixture, most researchers adopt the traditional image enhancement method. These enhancement methods usually include a series of operation procedures, each of which also requires the selection of processing thresholds. Such as the use of histogram equalization, brightness adjustment and filter filtering for image enhancement in the research of CT scan image of asphalt mixture damage [43]. In addition, noise reduction such as median filtering [18] and Gaussian filtering [44] have also been widely adopted. Furthermore, based on the local information of the image, some studies have used fuzzy mathematics to denoise the CT images. These image enhancement schemes can only meet single-stage image enhancement and reasonable threshold selection is required. In other words, they cannot meet the requirement of enhancing multiple number

of images by one single model. Therefore, there is an urgent demand of developing more effective and flexible solutions.

Intuitively, another way of improving the quality of CT images is to increase the intensity of scanning radiation source. As has been mentioned, sufficient radiation intensity is often required to obtain higher quality CT images. However, increasing the intensity of the radiation means higher experimental costs, which makes it difficult to carry out a large number of comparative experiments. Therefore, extensive studies on how to perform CT scans with low-intensity rays to obtain high-quality CT images is of great significance for reducing experimental costs.

In the field of medical image, convolutional autoencoder has been used for medical CT image denoising [45]. The residual encoder-decoder convolutional neural network is also used to perform the noise reduction process of CT images, and achieves a better noise reduction effect [15]. In addition, there are also studies that combine adversarial training to obtain image noise reduction models, in which the discriminator provides additional adversarial loss and the generator serves as the final noise reduction model [46]. Nevertheless, the characteristics of asphalt mixture CT images are very different from those of medical CT images, so the corresponding networks cannot be used directly. Moreover, most image enhancement only addresses the problem of image noise, but CT images of asphalt mixture also face problems such as blur and brightness discomfort.

In order to improve the imaging quality of CT images and reduce the cost of CT scanning, this paper proposes two adaptive image enhancement models combined with deep learning technology. Both models take into account image features and enhanced semantic features to achieve end-to-end image enhancement. To achieve high quality image enhancement, a model without semantic loss has been developed, which can achieve lossless embedding of semantic features. In order to achieve high flexibility of being able to adapt to different situations in real applications, a model with semantic loss was developed. This model can

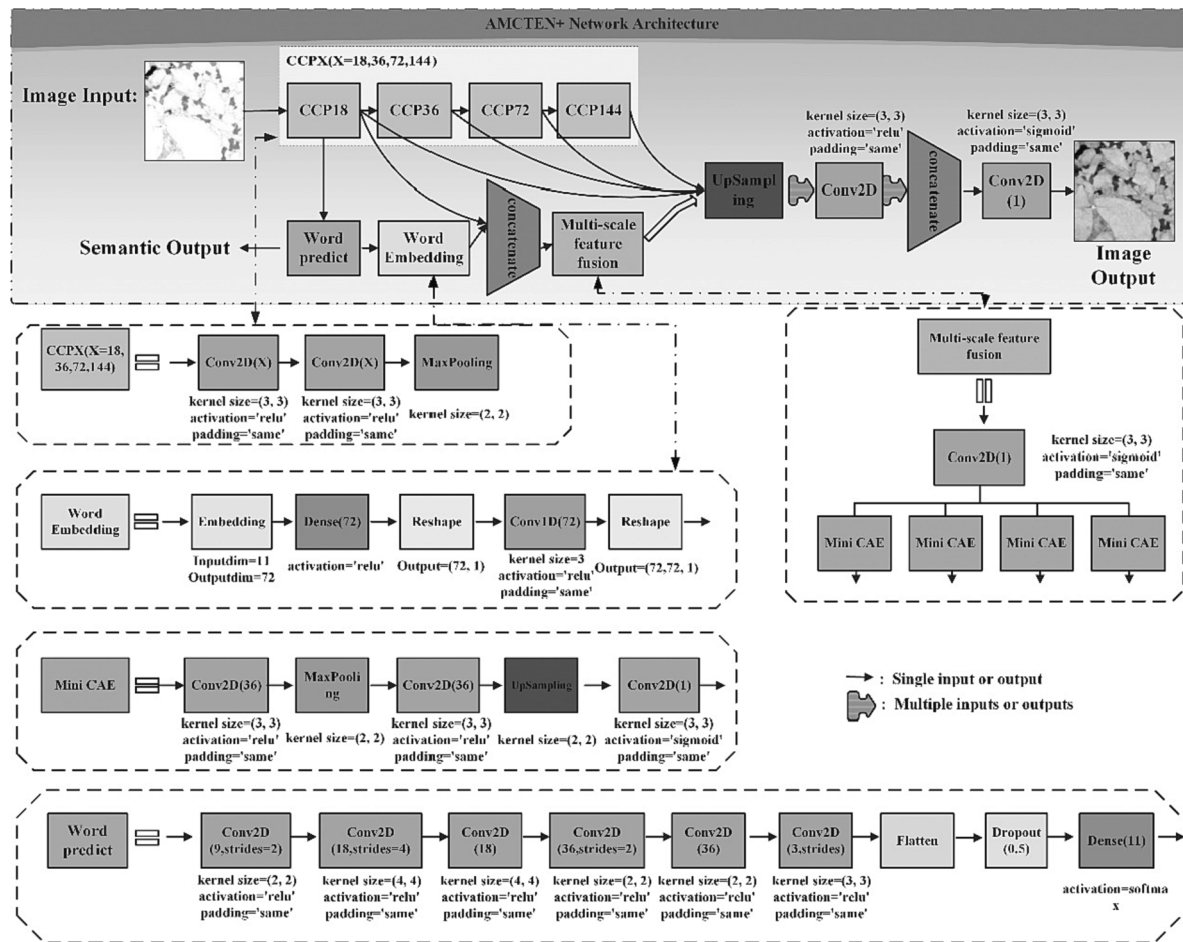


Fig. 5. AMCTEN + network architecture.

**Table 1**

Corruption strategies and corruption parameters.

Corruption Strategies	Corruption Parameters
Add noise (Gaussian)	$\mu = [0.1, 0.2]$
Blur image (Gaussian)	$\delta = [3, 3.1]$
Lighten(Gamma transform)	$\gamma = [0.4, 0.1]$
Darken(Gamma transform)	$\gamma = (1, 2.5]$

automatically select the enhancement scheme only by inputting images under the premise of losing some enhancement quality, which makes the processing more convenient.

## 2.2. Characteristics of asphalt mixture CT image

Unlike ordinary cameras that use light-sensitive components for imaging, CT equipment combines the principle of different ray attenuation of objects with different densities and the back projection method for image acquisition. The definition is expressed as follows:

$$I = I_0 e^{-\mu x} \quad (1)$$

where,  $I$  is the outgoing intensity,  $I_0$  is the incident intensity, and  $X$  is the traveling distance of ray. In this special image acquisition process, the image quality degradation comes from the tube current dissipation effect, the image transmission process and the electron beam intensity matching issues. For CT scanning of asphalt mixture, multiple images can be extracted from scanning a specimen, which are mainly gray scale images. Due to the different thickness of radiographic projection, the images at different positions of the same specimen have different

degrees of quality degradation.

## 3. Methodology

In order to enhance the asphalt mixture industry CT imaging quality, this paper proposes a CT image enhancement scheme based on fusion of semantic information. In the study, two kinds of information are provided for the training process of the model, which is semantic information and image information respectively. For the image information, it is the CT image of the asphalt mixture. On the other hand, semantic information indicates how the image needs to be repaired. Firstly, the original images of asphalt mixture with their semantic information is used as the input. Image features and semantic features are fused by several parallel Mini Convolution Auto Encoder (MiniCAE) modules. In this way, the model can adjust the image automatically according to the selected enhancement scheme. Furthermore, a new model has been provided. The new model can automatically recognize enhanced semantics information through the Word Pred block. This paper named first model as Asphalt Mixture CT Image Enhancement Network (AMCTEN), The second model as its plus version (AMCTEN + ). The first model aims to deal with the situation when semantic information is available, and when a lot of processing is required and semantic information is difficult to provide, the second model shows its value.

### 3.1. AMCTEN architecture

The structure AMCTEN is shown in Fig. 4. Feature Pyramid Networks (FPN) structure is selected as the image feature extraction network to obtain the feature maps of four sizes. Each unit consists of two

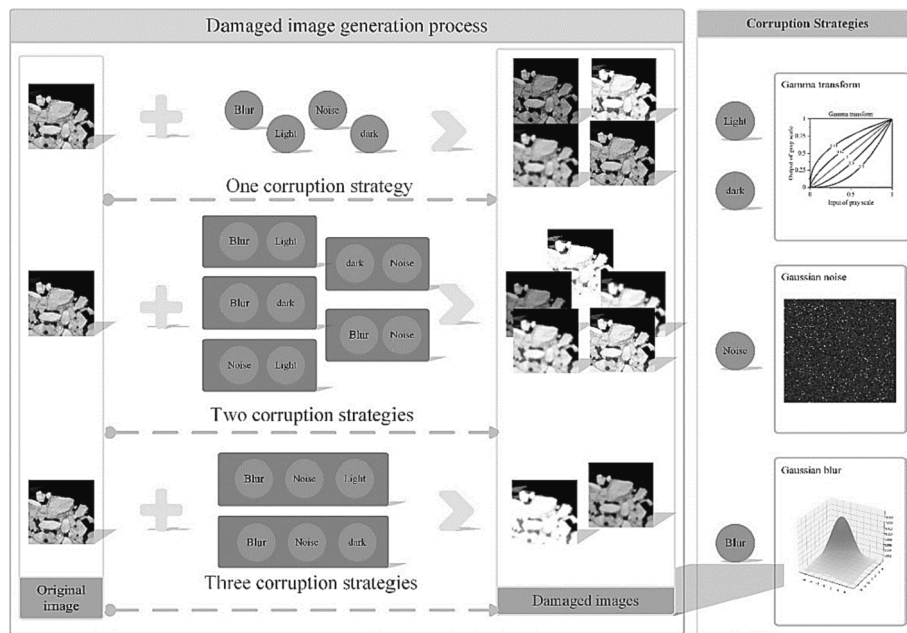


**Fig. 6.** Damaged image generation process.

convolutional layers and a max pooling layer, the convolutional layer convolution kernel size is  $3 \times 3$ , and the pooling layer convolution kernel size is  $2 \times 2$ . which is to maximize the information of input image features.

As can be seen from the architecture of AMCTEN, word embedding block is constructed to embed semantic features. Each semantic is represented as a 72-length vector. For the word embedding structure, first, 11 kinds of semantic information are compiled into vectors of length 72 through the embedding layer, and then through the fully connected layer, combined with Reshape to increase the dimension, then through one-dimensional convolution, and finally through the Reshape layer to obtain the feature map of word vectors. After that, a  $72 \times 72 \times 1$  semantic information feature map was obtained through a series of coding and dimension transformation. Several Mini CAE blocks are used in parallelly as the multi-scale feature fusion structure. Mini CAE is a smaller version of CAE, consisting of three convolutional layers, one downsampling layer and one upsampling layer. The outputs of multi-scale features are fused again with the image information extracted by FPN to obtain the final output result. These are implemented by a convolution with an output channel of 1. The corresponding Upsampling block in the AMCTEN has 8 inputs and 8 outputs. Different inputs correspond to different upsampling scales, but the output has the same size. These are determined by the convolution kernel size of the upsampling layer. The convolution kernel length and width used in this study is  $2 \times 2$ ,  $4 \times 4$ ,  $8 \times 8$  and  $16 \times 16$ .

### 3.2. AMCTEN + architecture

The architecture of AMCTEN + is shown in Fig. 5. The main framework of the model is the same as AMCTEN. The main difference is that this model uses Word Pred block to learn semantic information from the image. Intuitively, the semantic information of the image used as the input of Word Embedding block for subsequent feature processing. The main feature of this model is that it only requires for original CT image as the input, without adding additional semantic information, to get the final processing results. It should be mentioned that even though less information is required, this approach also introduces some semantic learning errors. As output features, semantic features are processed as 11-dimensional One-Hot vectors, which are smoothed. Word Pred block achieves fast image dimensionality reduction and output of multi-

classification results through a series of convolutions that control the step size. Through the Word Pred block method provided in this article, AMCTEN + only adds 10,000 to 20,000 parameters on the basis of AMCTEN, and achieves a higher accuracy. In addition, the parameters of the neural network in this study are obtained by the summary attribute of the instantiated network, which can display the total parameters of the neural network structure.

### 3.3. Training procedure

The operating system used in this experiment is Ubuntu 18.04.5. The model relies on TensorFlow 2.7.0. The GPU is GeForce RTX 3090. CPU version used in this research is Intel(R) Xeon(R) Gold 6226R CPU @ 2.90 GHz, with the Memory of 128G.

The optimization strategy is Adam when training models. The learning rate is 0.0001. Batch size is 8. A total of 20 epochs were trained.

#### 3.3.1. Loss function

The loss function used in the training of AMCTEN is expressed in Eq. (2).

$$L = \frac{1}{N} \sum_i L_i = \frac{1}{N} \sum_i -[y_i \log(p_i) + (1 - y_i) \log(1 - p_i)] \quad (2)$$

where  $y_i$  represents the label of sample i. If sample i belongs to the positive class, then  $y_i = 1$ , otherwise  $y_i = 0$ .  $p_i$  represents the probability that sample i is predicted to be a positive class; N represents the total number of samples.

For multiple categories, the categorical cross entropy as shown in Equation (3) has been used in to train the model.

$$L = \frac{1}{N} \sum_i L_i = -\frac{1}{N} \sum_i \sum_{c=1}^M y_{ic} \log(P_{ic}) \quad (3)$$

where  $y_{ic}$  represents the true classification of sample i. If the true type of sample i is equal to c, take 1, otherwise take 0;  $P_{ic}$  represents the probability that sample i is predicted to be c; M represents the number of classifications.

#### 3.3.2. Evaluation metric

In order to evaluate the CT image enhancement effect of asphalt

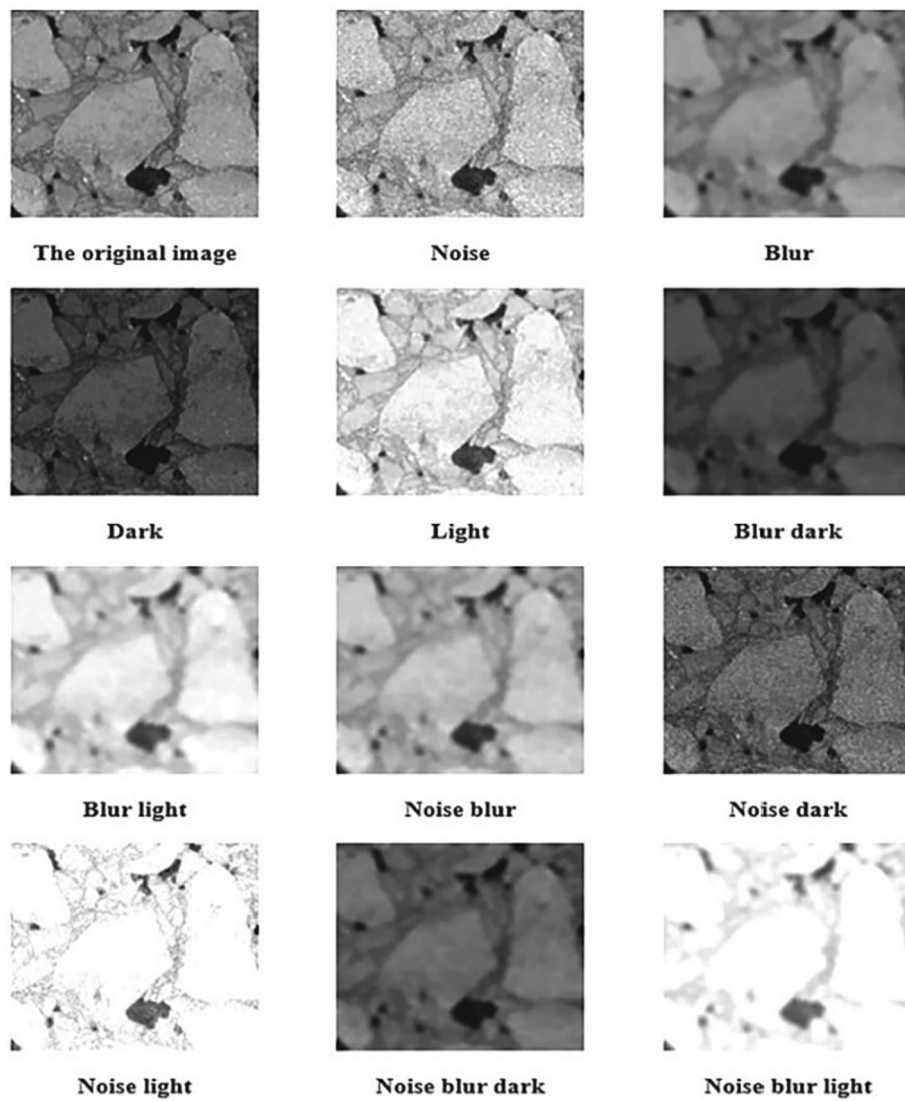


Fig. 7. CT image of asphalt mixture damaged by different strategies.

mixture, this study selected Peak signal to noise ratio (PSNR), Structural similarity (SSIM), and mean square error (MSE) to assess the models. Each calculation metric is defined as follows:

$$MSE = -\frac{i}{mm} \sum_{m=0}^{m-1} \sum_{n=0}^{n-1} h(x(i,j)) - Y(i,j)h^2 \quad (4)$$

where, X and Y represent the two images to be compared.

$$PSNR = 10 \cdot \log_{10} \left( \frac{MAX_X^2}{MSE} \right) = 20 \cdot \log_{10} \left( \frac{MAX_X}{\sqrt{MSE}} \right) \quad (5)$$

where, MAXX represents the largest gray value in the image. In this study, the value is 255.

SSIM index consists three different items each represents one aspect of the processed image, which are luminance L(X,Y), contrast C(X,Y) and structure S(X,Y). As shown in Eqs. (6)–(8).

$$L(X, Y) = \frac{2\mu_X\mu_Y + C_1}{\mu_X^2 + \mu_Y^2 + C_1} \quad (6)$$

$$C(X, Y) = \frac{2\sigma_X\sigma_Y + C_2}{\sigma_X^2 + \sigma_Y^2 + C_2} \quad (7)$$

$$S(X, Y) = \frac{\sigma_{XY} + C_3}{\sigma_X\sigma_Y + C_3} \quad (8)$$

where,  $\mu_X$  and  $\mu_Y$  denote the mean values of images X and Y respectively;  $\sigma_X$  and  $\sigma_Y$  represent the standard deviation of images X and Y respectively.  $\sigma_X^2$  and  $\sigma_Y^2$  represent the variance of images X and Y respectively.  $C_1$ ,  $C_2$  and  $C_3$  are constants. Furthermore, the SSIM can be calculated by Eq. (9).

$$SSIM(X, Y) = L(X, Y) * C(X, Y) * S(X, Y) \quad (9)$$

### 3.4. Dataset

Our dataset contains 6500 CT slice images. These images are selected from AC13, AC16 and AC20 graded asphalt mixtures, where the asphalt is base bitumen and the aggregate is limestone. These images were cut from original CT images of 516 pixels by 516 pixels. Each slice image is 144 pixels by 144 pixels for computational resource reasons. The ratio between training set, verification set and test set is 12:3:1.

In order to obtain low-quality CT images, this research randomly damage the original image by adding noise, blurring the image and adjusting brightness. The degree of adjustment is determined randomly. Gaussian additive noise is used for the addition of noise, and its formula is described as Eq. (10).

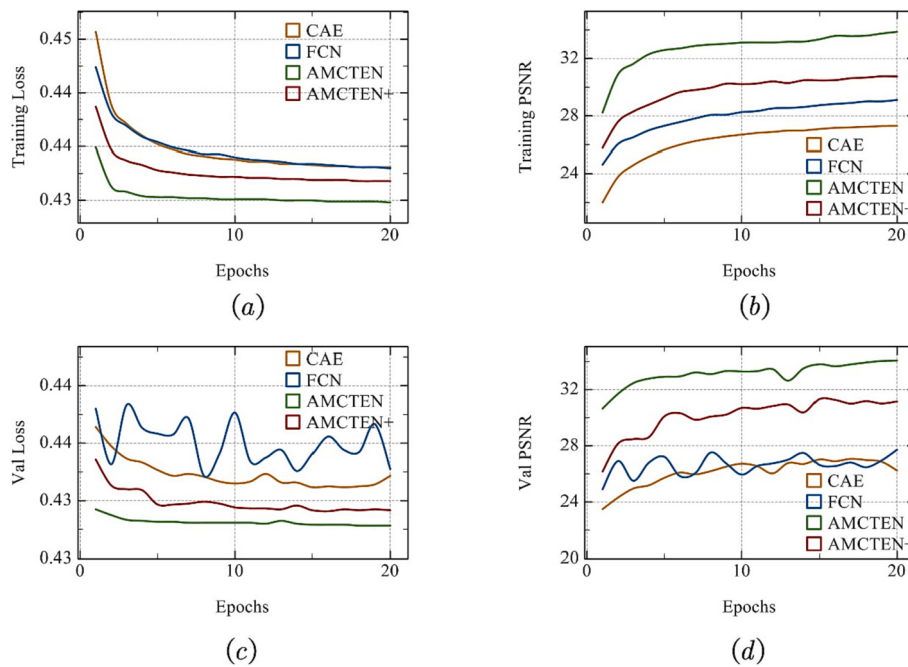


**Fig. 8.** The performance of training set and verification set in the training process. (a) Training set loss curve; (b) Training set PSNR curve; (c) Validation set loss curve; (d) Validation set PSNR curve.

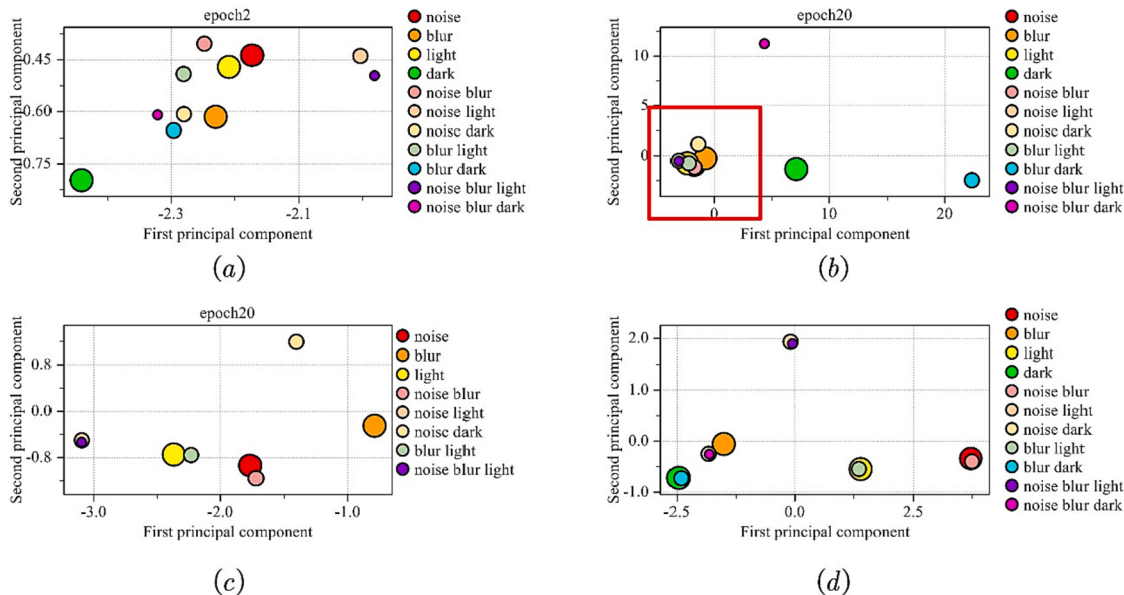


**Fig. 9.** PCA results. (a) Two times trained AMCTEN + model; (b) Twenty times trained AMCTEN+; (c) Zoomed in boxed information of b; (d) Twenty times trained AMCTEN.

**Table 2**

Evaluation of performance indicators for different models in test sets.

Model	Total params	PSNR		SSIM		MSE	
		Value(dB)	Increase rate (%)	Value	Increase rate (%)	Value	Decrease rate (%)
CAE	928,693	25.5	41.9	0.706	-8.7	234.4	89.3
FCN	614,475	27.9	55.7	0.793	2.6	150.2	93.1
AMCTEN	460,617	32.1	79.0	0.890	15.1	54.3	97.5
AMCTEN+	477,417	29.9	66.4	0.876	13.3	102.8	95.3
Damaged images	-	17.9	0.0	0.773	0.0	2190.2	0.0

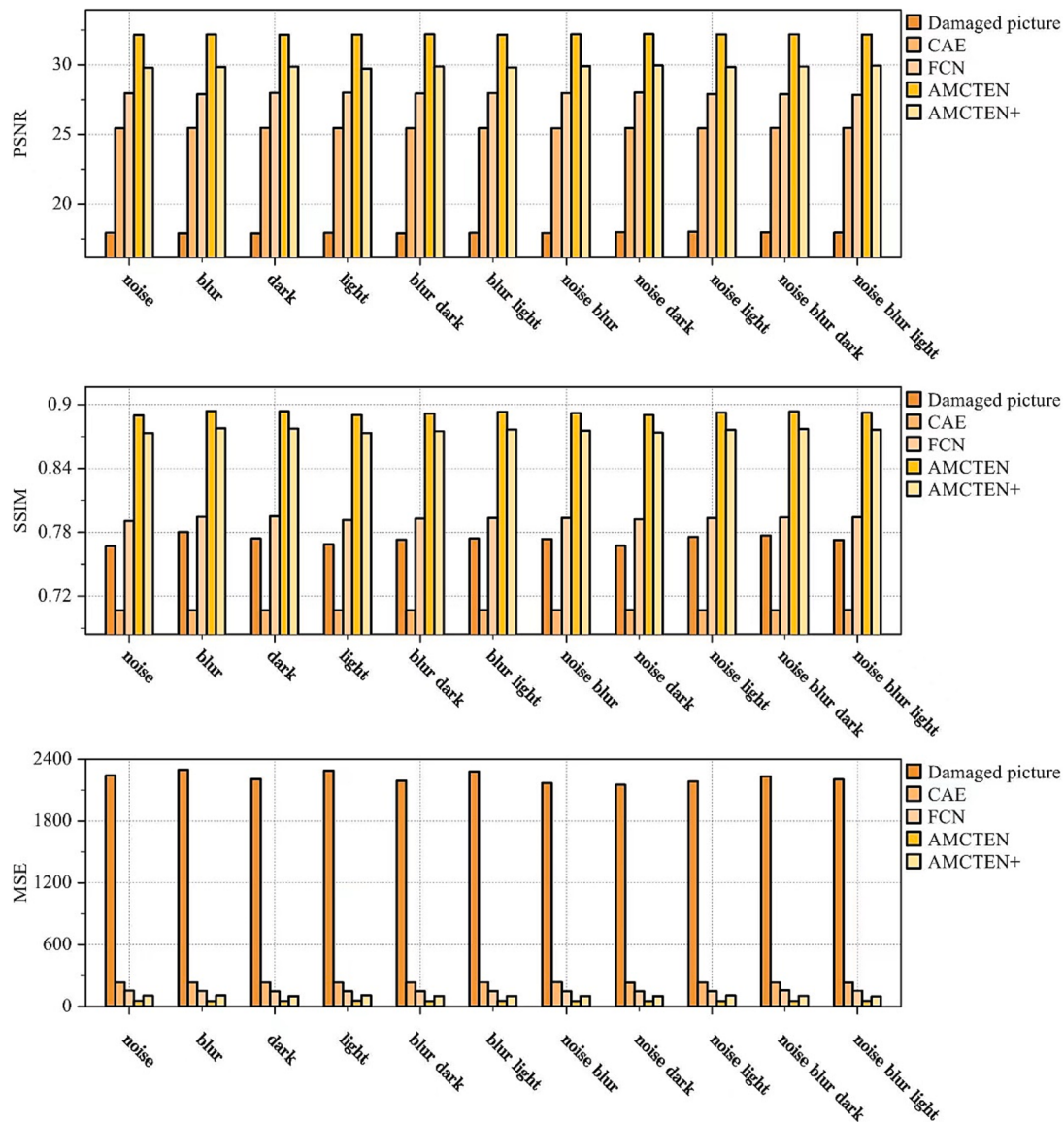


Fig. 10. The evaluation of each model in different image enhancement tasks in the test set.

$$F(x, y) = f(x, y) + (m + N^* \sigma) \quad (10)$$

where,  $N$  represents random numbers with Gaussian properties,  $m$  and  $\sigma$  mean gaussian distribution mean and variance,  $f$  means original image,  $F$  means the Image after adding noise.

Parameters related to damaged images are shown in the Table 1.

In the table,  $\mu$  represents the mean value of Gaussian noise,  $\sigma$  represents the variance of Gaussian fuzzy filter, and  $\gamma$  represents the parameter of Gamma transform.

As shown in Fig. 6, this research has divided corruption strategies into the following 11 categories: noise, blur, dark, light, blur-dark, blur-light, noise-blur, noise-dark, noise-light, noise-blur-dark, noise-blur-light.

The processing results are shown in Fig. 7. Considering that the combination of brightening and darkening is equivalent to one or the other, this research ignore the strategy containing both brightening and darkening. In order to expand the dataset, the above 11 transformations for each image in the dataset has been performed. After transformation, 52,800 images form the final training set.

#### 4. Experiments and analysis

In this study, Fully Convolutional Network (FCN) and Convolution Auto Encoder (CAE) models were used as the control group (without considering the input and output of semantic characteristics). Meanwhile, PSNR was selected as the evaluation index of the enhanced quality of asphalt mixture CT image. The performance is shown in the Fig. 8.

In general, AMCTEN has the best convergence effect and performance in both training and validation data sets, and AMCTEN+ is the second. This shows that considering semantic information simultaneously can improve the model's ability to handle multiple image enhancement tasks. In addition, AMCTEN performs better than AMCTEN+. This is because AMCTEN semantic information is directly input, whereas AMCTEN+ is trained. The semantic classification accuracy of AMCTEN+ verification set is about 0.9, indicating that the semantic information generated by AMCTEN+ contains a little noise. This semantic noise causes performance degradation of AMCTEN+.

To further analyze the semantic features, the word vectors generated by the two models are extracted. Through principal component analysis (PCA), the first principal component and the second principal

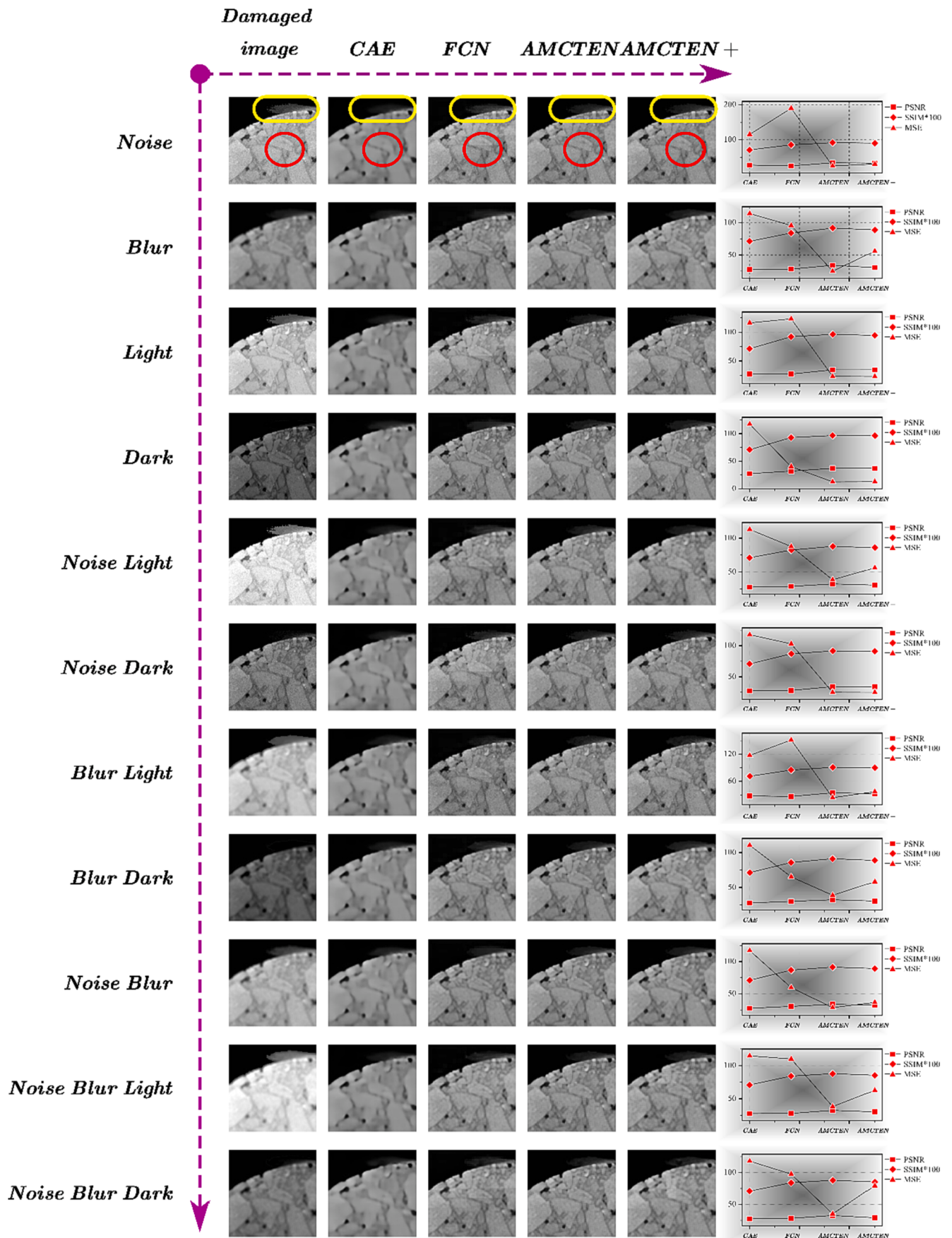
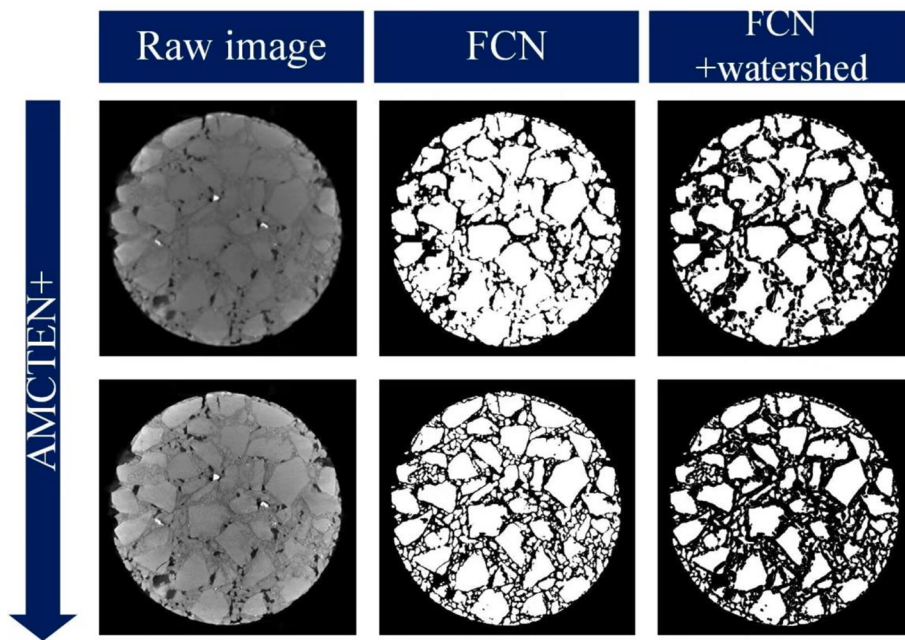


Fig. 11. Output effects of different image enhancement tasks under different models.



**Fig. 12.** Output effects of different image enhancement tasks under different models.

component are obtained of the embedded matrix.

In Fig. 9, three points of different sizes are used to represent different types of semantic features. Specially, the largest points represent single semantic feature, such as noise; the medium points represent double semantic features, such as noise-blur; and the smallest points represents multiple semantic features, such as a mixture of noise-blur-light. Fig. 9 (a) to (c) are the features of AMCTEN + embedding layer, and Figure (d) is the features of AMCTEN embedding layer. Observing Fig. 9(a) and (b), scattered semantic features gradually form specific semantic space with the progress of training. Therefore, the spatial structure of this model takes the correlation between different image enhancement tasks into account so that the final model can flexibly adapt to different image enhancement tasks with satisfactory performance.

Comparing Fig. 9 (b) to (d), it can be observed that the semantic feature distribution of the two models is different. There are two reasons for this. The first reason is that even for the same model, gradient descent does not converge to the same local optimal solution every time, which makes the embedding matrix different. The second reason is that the semantic feature input of AMCTEN + is obtained through training, which makes the semantic feature input noisy. The network corrects the embedding matrix to improve the image output quality.

However, even though the semantic features have different distributions, semantic features still reflect a certain degree of similarity. Semantic feature pairs such as (noise, noise-blur), (light, blur light) and (noise light, noise blur light) show similar proximity both in AMCTEN and AMCTEN +. Semantic features of the same level are separated from each other, and semantic features of different levels contain adjacent relations. This shows that word embedding can better reflect the interrelation between semantics than the embedding with One-hot encoding directly.

As shown in Table 2, the test results of the models are compared with two widely use models, which are CAE and FCN. Performance indicators include PSNR, SSIM, and MSE.

The increase or decrease rate of each indicator in the table describes the change rate of the output with respect to the damaged image.

The table shows that all the four models have improved the quality of CT image of asphalt mixture to some extent. The SSIM of CAE model was decreased. The reason is that CAE uses full convolutional connections which fails to consider the detailed features of the shallow feature maps, resulting in a loss of details. On the test set, the principle of AMCTEN >

AMCTEN+ > FCN > CAE can be obviously observed. For example, PSNR has increased 79.0 % and 66.4 % for AMCTEN and AMCTEN+, respectively, which were compared with 41.9 % (CAE) and 55.7 % (FCN). At the same time, both the quantity of parameters and size of the model have sequence of AMCTEN < FCN < CAE. This shows that considering semantic information when processing a variety of image enhancement tasks, AMCTEN and AMCTEN + can obtain higher quality with fewer parameters. In addition, the parameters in Table 2 reflect the efficiency of the model. Since the parameter quantities are all in the same order of magnitude, their inference speeds are roughly equivalent. The calculation speed of each image is about 3 s.

Moreover, this paper analyzed the stability of the model when dealing with different image enhancement tasks, and compared the processing results of 11 tasks based on Evaluation metric, as shown in the Fig. 10 and Fig. 11. the performance of different models under various image enhancement tasks. They all show the law of AMCTEN > AMCTEN+ > FCN > CAE in the enhancement of quality. This shows good stability of AMCTEN in different enhancement tasks of CT image of asphalt mixture. The image quality can be improved more effectively within the scope of the enhancement task set in this research.

As shown in the Fig. 12, the study combined FCN neural network to further extract aggregate features, and compared the segmentation results before and after enhancement. In the figure, the first column is the original image and the enhanced image. The second column is the aggregate image extracted by FCN. The third column combines the watershed algorithm for post-processing. After comparison, it can be seen that a large number of adhesion areas appearing in the segmentation before enhancement are more clearly distinguished after data enhancement. This also proves the effectiveness of the proposed algorithm.

## 5. Conclusion

To achieve automatically restore asphalt mixture images scanned by CT and reduce the experimental cost. This research combines deep learning technology to propose a CT image enhancement solution for asphalt mixture. The proposed method solves multiple image enhancement problems adaptively and improves the quality of the output image. The solution combines semantic information to solve multiple image enhancement problems at the same time. The main research conclusions

are as follows:

- (1) This study proposed two models to solve the CT image enhancement problem of asphalt mixture. The first model, AMCTEN, takes semantic information as input, and is suitable for obtaining higher image quality when image processing schemes are known. The second model, AMCTEN+, takes semantic information as the output, which is suitable for situations where the semantic information is unknown, and is more convenient to process.
- (2) Combined with experiments, it is proved that directly providing semantic features in AMCTEN can obtain higher image quality, and AMCTEN + has a slight decrease in image quality due to semantic loss.
- (3) This paper analyzes the semantic feature space of the model, points out the difference and similarity of the semantic feature of the model construction.
- (4) Combined with the verification on the test set, the model proposed in this paper is stable in performance for different image enhancement tasks.

However, this study provides two models to solve the problems of repair effect and repair efficiency, and it still has great research value to solve these two problems simultaneously with a single model. In addition, the diversity of datasets also restricts the scope of application of the model. In order to better improve image quality and conduct data analysis, in the next step, we will continue to improve in three aspects: obtaining higher quality original data images, reducing semantic learning loss, and realizing end-to-end image enhancement and image segmentation process.

#### CRediT authorship contribution statement

**Handuo Yang:** Conceptualization, Methodology, Investigation, Data curation, Writing – original draft, Validation. **Ju Huyan:** Conceptualization, Methodology, Supervision, Validation, Writing – review & editing, Funding acquisition. **Tao Ma:** Supervision, Methodology, Writing – review & editing, Funding acquisition. **Zheng Tong:** Methodology, Writing – review & editing. **Chengjia Han:** Methodology. **Tianyan Xie:** Methodology.

#### Declaration of Competing Interest

The authors declare that they have no known competing financial interests or personal relationships that could have appeared to influence the work reported in this paper.

#### Data availability

Data will be made available on request.

#### Acknowledgment

The authors would like to thank the anonymous referees for constructive comments. This study was supported by the financial support of National Key R & D program of China (Grant Number: 2021YFB2600600, 2021YFB2600604), National Natural Science Foundation of China (52108403), and the Fundamental Research Funds for the Central University of China (grant number: 2242022R10054).

#### References

- [1] T. Chen, T. Ma, X.M. Huang, S.J. Ma, F.L. Tang, S.P. Wu, Microstructure of synthetic composite interfaces and verification of mixing order in cold-recycled asphalt emulsion mixture, *J. Cleaner Prod.* 263 (2020).
- [2] X.H. Ding, L.C. Chen, T. Ma, H.X. Ma, L.H. Gu, T. Chen, Y. Ma, Laboratory investigation of the recycled asphalt concrete with stable crumb rubber asphalt binder, *Constr. Build. Mater.* 203 (2019) 552–557.
- [3] J.Y. Hu, T. Ma, K. Ma, DEM-CFD simulation on clogging and degradation of air voids in double-layer porous asphalt pavement under rainfall, *J. Hydrol.* 595 (2021).
- [4] S. Han, P. Sun, T.F. Fwa, Relationships between internal structure and surface texture of asphalt mixtures, *Road Mater. Pavement Des.* 22 (4) (2021) 894–909.
- [5] J.Q. Zhu, J.T. Zhong, T. Ma, X.M. Huang, W.G. Zhang, Y. Zhou, Pavement distress detection using convolutional neural networks with images captured via UAV, *Autom. Constr.* 133 (2022).
- [6] J.D. Huang, J. Zhang, J.L. Ren, H.W. Chen, Anti-rutting performance of the damping asphalt mixtures (DAMs) made with a high content of asphalt rubber (AR), *Constr. Build. Mater.* 271 (2021).
- [7] X.H. Ding, T. Ma, W.G. Zhang, D.Y. Zhang, T. Yin, Effects by property homogeneity of aggregate skeleton on creep performance of asphalt concrete, *Constr. Build. Mater.* 171 (2018) 205–213.
- [8] H. Jahanbakhsh, M.M. Karimi, H. Naseri, F. Moghadas Nejad, Sustainable asphalt concrete containing high reclaimed asphalt pavements and recycling agents: performance assessment, cost analysis, and environmental impact, *J. Cleaner Prod.* 244 (2020).
- [9] C.Y. Kuo, R.B. Freeman, C. Natl Res, C. Natl Res, C., Natl Res, Image analysis evaluation of aggregates for asphalt concrete mixtures, *Applications of Emerging Technologies, Transportation* (1998) 65–71.
- [10] C.J. Han, T. Ma, J. Huyan, X.M. Huang, Y.N. Zhang, CrackW-Net: A Novel Pavement Crack Image Segmentation Convolutional Neural Network, *Ieee Transactions on Intelligent Transportation Systems*.
- [11] P. Georgiou, C. Plat, Microstructure characterisation of field and laboratory roller compacted asphalt mixtures, *Road Mater. Pavement Des.* 22 (4) (2021) 942–953.
- [12] L.W. Shi, D.Y. Wang, J.F. Wang, Z.H. Jiang, H.H. Liang, X. Qin, A New Method for Designing Dense Skeleton Asphalt Mixture Based on Meso Parameter, *Adv. Civ. Eng.* 2020 (2020).
- [13] N. Brahmajaree, K. Kanitpong, A. Sawangsuriya, Investigation on internal structural properties of asphalt mixtures subjected to loading using image analysis, *Int. J. Pavement Eng.* 23 (1) (2022) 107–120.
- [14] H.M.Z. Hassan, K.H. Wu, W.K. Huang, S.H. Chen, Q.R. Zhang, J.W. Xie, X. Cai, Study on the influence of aggregate strength and shape on the performance of asphalt mixture, *Constr. Build. Mater.* 294 (2021).
- [15] L. Gao, Z.Q. Wang, Y.P. Liu, J.Q. Zheng, H. Li, Influence of Binder Property and Mortar Thickness on High-Temperature Performance of Cold Recycled Mixtures with Asphalt Emulsion, *Materials* 12 (17) (2019).
- [16] J.Y. Huang, J.Z. Pei, Y. Li, H.Y. Yang, R. Li, J.P. Zhang, Y. Wen, Investigation on aggregate particles migration characteristics of porous asphalt concrete (PAC) during vibration compaction process, *Constr. Build. Mater.* 243 (2020).
- [17] C. Du, P.F. Liu, Q. Liu, S. Leischner, Y.R. Sun, J.Y. Chen, M. Oeser, Development of locally homogeneous finite element model for simulating the mesoscale structure of asphalt mixture, *Comput. Struct.* 248 (2021).
- [18] F.B. Chen, B. Xu, H.Z. Jiao, X.M. Chen, Y.L. Shi, J.X. Wang, Z. Li, Triaxial mechanical properties and microstructure visualization of BFRC, *Constr. Build. Mater.* 278 (2021).
- [19] C. Du, P.F. Liu, Y.R. Sun, J.Y. Chen, Q. Liu, M. Oeser, Characterizing asphalt mixtures with random aggregate gradations based on the three-dimensional locally homogeneous model, *Computer-Aided Civil and Infrastructure Engineering*.
- [20] H.C. Dan, D. Yang, L.H. Zhao, S.P. Wang, Z. Zhang, Meso-scale study on compaction characteristics of asphalt mixtures in Superpave gyratory compaction using SmartRock sensors, *Constr. Build. Mater.* 262 (2020).
- [21] L.X. Fu, H.Y. Zhou, J. Yuan, W.L. An, X.H. Chen, Damage Fracture Characterization of Asphalt Mixtures Considering Freeze-Thaw Cycling and Aging Effects Based on Acoustic Emission Monitoring, *Materials* 14 (20) (2021).
- [22] K.A. Ahmad, N.A. Hassan, M.E. Abdullah, M.A.M. Bilema, N. Usman, A.M. Al Allam, M.r., Bin Hainin, Image processing procedure to quantify the internal structure of porous asphalt concrete, *Multidiscipline Model. Mater. Struct.* 15 (1) (2019) 206–226.
- [23] J.B. Krol, R. Khan, A.C. Collop, The study of the effect of internal structure on permeability of porous asphalt, *Road Mater. Pavement Des.* 19 (4) (2018) 935–951.
- [24] Y. Lei, H.N. Wang, Z.P. You, C.J. Ji, S. Dong, X. Yang, J.F. Gao, J.K. Xiao, Effect of Key Aggregate Morphology and Mold Modulus on the Spatial Distribution of Internal Air Voids in the Compacted Asphalt Mixture, *J. Test. Eval.* 48 (6) (2020) 4324–4342.
- [25] P.D. Cui, S.P. Wu, Y. Xiao, Y.Y. Niu, G.M. Yuan, J.T. Lin, 3D reconstruction of moisture damage resulted volumetric changes in porous asphalt mixture, *Constr. Build. Mater.* 228 (2019).
- [26] G. Xu, Y.H. Yu, D.G. Cai, G.Y. Xie, X.H. Chen, J. Yang, Multi-scale damage characterization of asphalt mixture subject to freeze-thaw cycles, *Constr. Build. Mater.* 240 (2020).
- [27] P.L. Li, J.F. Su, P. Gao, X. Wu, J.G. Li, Analysis of aggregate particle migration properties during compaction process of asphalt mixture, *Constr. Build. Mater.* 197 (2019) 42–49.
- [28] T.S. Li, P.F. Liu, C. Du, M. Schnittcher, J. Hu, D.W. Wang, M. Oeser, Microstructural analysis of the effects of compaction on fatigue properties of asphalt mixtures, *Int. J. Pavement Eng.* 23 (1) (2022) 9–20.
- [29] W.L. Wu, Z. Li, X.N. Zhang, M.H. Li, Evaluating RLWT Rutting Test of Asphalt Mixtures Based on Industrial Computerized Tomography, *Adv. Mater. Sci. Eng.* 2018 (2018).

- [30] J.J. Wei, H.B. Li, C. Wan, Experimental Evaluation of X-ray CT Images of Asphalt Mixture Based on Threshold Segmentation Principle, 3rd International Conference on Manufacturing Science and Engineering (ICMSE 2012), Xiamen, PEOPLES R CHINA, 2012, pp. 327-+.
- [31] J.T. Zhang, J. Yang, T.J. Liu, R.X. Cai, R. Yang, Study on Void Structure Reconstruction of Asphalt Mixture by X-Ray Computed Tomography and Otsu's Method, *Adv. Mater. Sci. Eng.* 2020 (2020).
- [32] J. Hu, P.F. Liu, D.W. Wang, M. Oeser, Influence of aggregates' spatial characteristics on air-voids in asphalt mixture, *Road Mater. Pavement Des.* 19 (4) (2018) 837–855.
- [33] W.K. Huang, Z.B. Ren, X.N. Zhang, J.M. Yu, Investigation on Microstructural Damage Properties of Asphalt Mixture Using Linear and Damage-Coupled Viscoelastic Model, *Appl. Sci. Basel* 9 (2) (2019).
- [34] C. Xing, H.N. Xu, Y.Q. Tan, X.Y. Liu, C.H. Zhou, T. Scarpas, Gradation measurement of asphalt mixture by X-Ray CT images and digital image processing methods, *Measurement* 132 (2019) 377–386.
- [35] H.C. Dan, G.W. Bai, Z.H. Zhu, Application of deep learning-based image recognition technology to asphalt-aggregate mixtures: Methodology, *Constr. Build. Mater.* 297 (2021).
- [36] N. Hasheminejad, G. Pipintakos, C. Vuyte, T. De Kerf, T. Ghalandari, J. Blom, W. Van den Bergh, Utilizing deep learning and advanced image processing techniques to investigate the microstructure of a waxy bitumen, *Constr. Build. Mater.* 313 (2021).
- [37] J.W. Jiang, Z. Zhang, Q. Dong, F.J. Ni, Characterization and identification of asphalt mixtures based on Convolutional Neural Network methods using X-ray scanning images, *Constr. Build. Mater.* 174 (2018) 72–80.
- [38] A.J. Enriquez-Leon, T.D. de Souza, F.T.S. Aragao, D. Braz, A.M.B. Pereira, L.P. Nogueira, Determination of the air void content of asphalt concrete mixtures using artificial intelligence techniques to segment micro-CT images, *International Journal of Pavement Engineering*.
- [39] S. Lefkimmatis, Ieee, Universal Denoising Networks : A Novel CNN Architecture for Image Denoising, 31st IEEE/CVF Conference on Computer Vision and Pattern Recognition (CVPR), Salt Lake City, UT, 2018, pp. 3204-3213.
- [40] J. Lehtinen, J. Munkberg, J. Hasselgren, S. Laine, T. Karras, M. Aittala, T. Aila, Noise2Noise: Learning Image Restoration without Clean Data, 35th International Conference on Machine Learning (ICML), Stockholm, SWEDEN, 2018.
- [41] K. Zhang, W.M. Zuo, Y.J. Chen, D.Y. Meng, L. Zhang, Beyond a Gaussian Denoiser: Residual Learning of Deep CNN for Image Denoising, *IEEE Trans. Image Process.* 26 (7) (2017) 3142–3155.
- [42] P.J. Liu, H.Z. Zhang, K. Zhang, L. Lin, W.M. Zuo, Ieee, Multi-level Wavelet-CNN for Image Restoration, IEEE/CVF Conference on Computer Vision and Pattern Recognition (CVPR), Salt Lake City, UT, 2018, pp. 886-895.
- [43] S.W. Zhang, X.N. Zhang, Z.Y. Wu, L.W. Shi, Research on Asphalt Mixture Injury Digital Image Based on Enhancement and Segmentation Processing Technology, 2nd International Conference on Mechanical Engineering, Materials Science and Civil Engineering (ICMEMSCE 2013), Beijing, PEOPLES R CHINA, 2013, pp. 832-837.
- [44] A.E. Calistru, G.J.B.o.U.o.A.S. Jităreanu, V.M.C.-N. Agriculture, Applications of X-Ray Computed Tomography for Examining Soil Structure: A Review, 72(1) (2015).
- [45] L. Gondara, Medical image denoising using convolutional denoising autoencoders, 16th IEEE International Conference on Data Mining (ICDM), SPAIN, Barcelona, 2016, pp. 241–246.
- [46] J.M. Wolterink, T. Leiner, M.A. Viergever, I. Isgrum, Generative Adversarial Networks for Noise Reduction in Low-Dose CT, *IEEE Trans. Med. Imaging* 36 (12) (2017) 2536–2545.